The Uncombed Penumbra

J. M. Borrero and M. Rempel

High Altitude Observatory, National Center for Atmospheric Research,[1]
P.O. Box 3000, Boulder, CO 80307-3000, U.S.A.

S. K. Solanki

Max-Planck-Institut für Sonnensystemforschung, Max-Planck-Strasse 2,
D-37191 Katlenburg-Lindau, Germany

Abstract. The uncombed penumbral model explains the structure of the sunspot penumbra in terms of thick magnetic fibrils embedded in a surrounding, magnetic atmosphere. This model has been successfully applied to explain the polarization signals emerging from the sunspot penumbra. Thick penumbral fibrils face some physical problems, however. In this contribution we will offer possible solutions to these shortcomings.

1. Introduction

The structure of the penumbra has been a subject of intensive research in the last years. Most of our current knowledge is based on the interpretation of the polarized line profiles that carry useful information about the magnetic field topology. A consistent picture of the sunspot penumbra, able to explain the various observations available at different wavelengths, spatial resolutions, etc., has not yet emerged (Solanki 2003).

A widely used model is the so-called "uncombed penumbral model" by Solanki & Montavon (1993). It is based on the idea of a penumbra consisting of highly inclined magnetic flux tubes[2] embedded in a more vertical magnetic background (for practical implementations a simplified version is used: see Borrero et al. 2003, 2005). This model has been especially successful in explaining a number of key observations:

- it reproduces the properties (magnitude, sign, distribution, and center-to-limb variation) of the Net Circular Polarization (NCP) observed in the sunspot penumbra in the visible Fe I lines at 6301 Å (Solanki & Montavon 1993; Martínez Pillet 2000) and in the Fe I lines at 1.56 μm (Schlichenmaier & Collados 2002; Schlichenmaier et al. 2002; Müller et al. 2002).

---

[1]National Center for Atmospheric Research is sponsored by the National Science Foundation.

[2]In this paper we will use indistinctly the term magnetic fibril or magnetic flux tube. Note that as a matter of fact the fibrils correspond to an anti-flux tube since its magnetic field strength is smaller that in the magnetic surrounding atmosphere (see Fig. 6 in Borrero et al. 2005).

- it offers an explanation for the opposite vertical gradients (in the line-of-sight velocity, magnetic field inclination, and magnetic field strength) obtained from the inversion of spectro-polarimetric data of the spectral lines, when different spectral lines are used (Westendorp Plaza et al. 2001a,b; Mathew et al. 2003; Borrero et al. 2004).

- it consistently reproduces the polarization signals that emerge from the sunspot penumbra in a variety of spectral lines and sunspots at different heliocentric angles (Borrero et al. 2005, 2006).

- it retrieves flux tubes whose vertical extension is about 100–300 km (see left panel in Fig. 1). This is comparable to the horizontal extension seen in high resolution continuum images (Scharmer et al. 2002; Rouppe van der Voort et al. 2004; Sütterlin, Bellot Rubio, & Schlichenmaier 2004).

In addition to this, numerical simulations of thin penumbral flux tubes are able to explain the proper movements of the penumbral grains and moving magnetic features (Schlichenmaier 2002), as well as various features of the Evershed flow (Thomas & Montesinos 1993; Montesinos & Thomas 1997; Schlichenmaier, Jahn, & Schmidt 1998a,b).

The magnetic topology inferred from the application of the uncombed model to spectro-polarimetric observations is very similar to that used in numerical simulations of penumbral flux tubes. The main difference lies in the vertical extension of the penumbral fibrils. While numerical simulations consider those flux tubes to be thin (much smaller than the typical pressure scale height), spectro-polarimetric observations indicate that this might not be the case. Note that from the inversion of Stokes profiles it is not possible to distinguish between a thick flux tube or a bundle of thin flux tubes next to each other (see discussion in Borrero et al. 2006).

In the *thin* case, numerical simulations would have problems offering an explanation for the heating and brightness of the penumbra (Schlichenmaier & Solanki 2003; Spruit & Scharmer 2006). Even if the flux tube carries hot plasma at, say, 12000 K, it cools down so fast (Schlichenmaier, Bruls, & Schüssler 1999) that the only possibility left is either that the flux tube is thick (in order to increase the cooling time) or that there are many thin flux tubes per resolution element that carry hot plasma upflows into the penumbra, cool down, and sink again into deeper layers within the same resolution element. Rouppe van der Voort et al. (2004) and Langhans et al. (2005) observe long lived (~ 1 h) penumbral filaments that are highly coherent over portions of the penumbra of several thousand kilometers. This seems to rule out the last possibility. We therefore turn our attention to the *thick* case: flux tubes with 100–300 km diameter.

2.   Problems in Embedded Thick Flux Tubes

When a horizontal (initially homogeneous) magnetic flux tube $\boldsymbol{B}_{\rm t}$ is embedded in an external vertical magnetic field $\boldsymbol{B}_{\rm s}$, this external or surrounding field has to bend sideways in order to accommodate the flux tube. A situation like this is depicted in Fig. 2 (Case A). The component of the magnetic field vector along the direction perpendicular to the flux tube's surface vanishes for both the flux
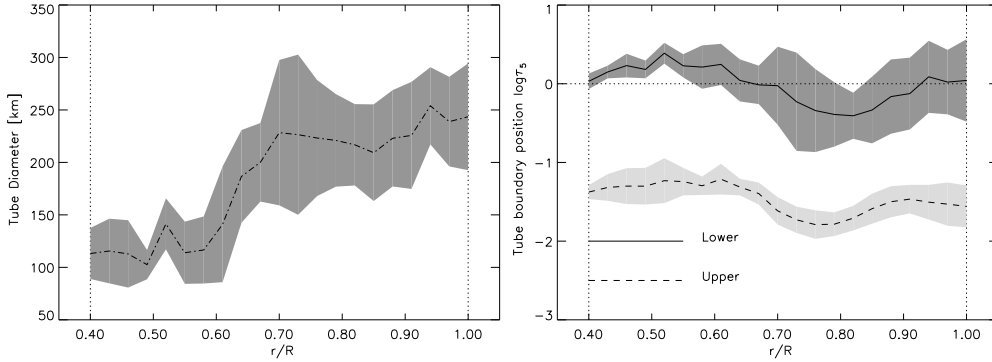
Figure 1.   *Left:* flux tube diameter as a function of the sunspot normalized radial distance in the penumbra. *Right:* radial variation of the lower (solid line) and upper (dashed) flux tube's boundaries in the optical depth scale (both figures from Borrero et al. 2006).
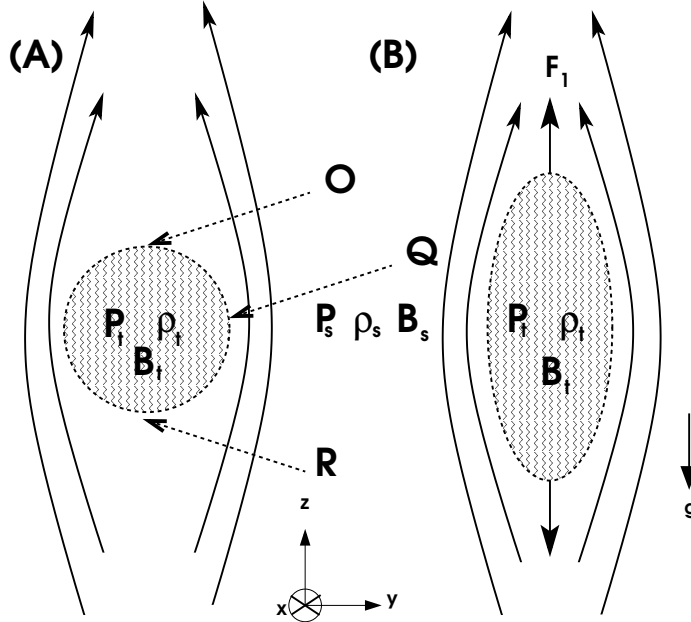

Figure 2.   *Left:* Case A. A homogeneous flux tube with density ρ_t and pressure P_{t} and horizontal (with respect to the vertical in the solar surface) magnetic field $\boldsymbol{B}_{\mathrm{t}} = (B_{\mathrm{t}x}, 0, 0)$, is placed in a homogeneous environment with ρ_{s} and P_{s} where the magnetic field is vertical, $\boldsymbol{B}_{\mathrm{s}} = (0, B_{\mathrm{s}y}, B_{\mathrm{s}z})$. *Right:* Case B. The external field lines bend around the flux tube, creating tension forces that stretch the flux tube vertically.

tube and surrounding field. This leads to total pressure balance between them,

$$P_{\mathrm{t}}^{*} + \frac{B_{\mathrm{t}}^{2*}}{8\pi} = P_{\mathrm{s}}^{*} + \frac{B_{\mathrm{s}}^{2*}}{8\pi} \; , \tag{1}$$

where the symbol * indicates the boundary or interface between the flux tube and the surrounding, magnetic atmosphere. At the sides of the flux tube (point Q in Fig. 2) we have

$$P_{\mathrm{t}} - P_{\mathrm{s}} = \frac{B_{\mathrm{s}z}^2 - B_{\mathrm{t}x}^2}{8\pi} \ , \tag{2}$$

while at the top and at the bottom of the flux tube (points O and R in Fig. 2), since the external magnetic field vanishes completely, we have

$$P_{\mathrm{t}} - P_{\mathrm{s}} = -\frac{B_{\mathrm{t}x}^2}{8\pi} \ . \tag{3}$$

Any $P_{\mathrm{t}} - P_{\mathrm{s}}$ that balances Eq. (2) unbalances Eq. (3) in the amount of $B_{\mathrm{s}z}^2/8\pi$. This imbalance induces net forces at the top and at the bottom of the flux tube, which tend to stretch it vertically,

$$\boldsymbol{F}_1^{\mathsf{O}} = \frac{B_{\mathrm{s}z}^2}{8\pi R}\, \boldsymbol{e}_z \ , \tag{4}$$

$$\boldsymbol{F}_1^{\mathsf{R}} = -\frac{B_{\mathrm{s}z}^2}{8\pi R}\, \boldsymbol{e}_z \ . \tag{5}$$

These forces cause the flux tube to expand vertically in a time scale of

$$t_{\mathrm{expan}} = \frac{l}{v} \sim \frac{R}{v_a} \sim \frac{R}{B}\sqrt{4\pi\rho} \sim 20\,\mathrm{s} \ , \tag{6}$$

where we assumed a flux tube radius of $R = 100\,\mathrm{km}$, a typical density of $\rho = 3 \times 10^{-7}\,\mathrm{g\,cm^{-3}}$, and a field strength of $B = 1000\,\mathrm{G}$.

If nothing stops this process, the flux tube upper boundary will indefinitely move upwards and the bottom one will move downwards (see Case B in Fig. 2). This will end up breaking our idea of flux tube and of uncombed penumbra, since the gradients at the flux tube's boundaries (needed in the uncombed model to create NCP) will disappear from the regions in which the spectral lines are formed.[3] In the following we consider if this stretching process is bounded.

3.   Flux Tubes in Convectively Stable Layers

Let us assume that the upper part of our initially homogeneous flux tube rises from a height z_0 to a height z, as a consequence of the vertical stretching previously discussed. If the atmosphere is sub-adiabatic (super-adiabatic index $\delta < 0$), a restoring force will try to bring back the flux tube to its original position z_0,

$$\boldsymbol{F}_2^{\mathsf{O}} = \frac{\rho g \delta \Delta z}{H_{\mathrm{p}}}\, \boldsymbol{e}_z \ , \tag{7}$$

---

[3]Note that the mentioned stretching applies to both thick and thin flux tubes as long as they are embbeded in a surrounding, magnetic atmosphere. However, the problem with the tube's boundaries (moving out of the region in which the spectral lines are formed) is more likely to happen in the thick case.

where $H_\mathrm{p} = P/(\rho g)$ is the pressure scale height. Note that $\boldsymbol{F}_2^\mathsf{O}$ opposes $\boldsymbol{F}_1^\mathsf{O}$ (see Eq. [4]) since $\Delta z > 0$ and $\delta < 0$. The main question is how much the upper portions of the flux tube can rise before the anti-buoyant restoring force compensates the magnetic forces. This can be estimated by comparing Eq. (4) and Eq. (7),

$$\frac{\Delta z}{H_\mathrm{p}} = -\frac{B_{\mathrm{s}z}^2}{8\pi R\rho g}\frac{1}{\delta} \sim -\frac{0.75}{\delta} \ . \tag{8}$$

Using $\delta = -0.4$ (ideal gas at a constant temperature; see Moreno-Insertis & Spruit 1989) and $B_{\mathrm{s}z} = 1250\,\mathrm{G}$, we deduce that the vertical stretching occurring in the upper region of the flux tube is of the order of one or two pressure scale heights, $\Delta z \sim H_\mathrm{p} = P/(\rho g) \sim 100\text{--}200\,\mathrm{km}$. At this height its density will be $1 - \delta$ times the density of the surrounding, magnetic atmosphere.

This value for the vertical stretching is at the limits of what is needed to keep the flux tube boundary within the spectral line forming region. Futhermore, these estimates were done for the case of the top and bottom of the flux tube. As we move towards the sides (point Q in Fig. 2) the vertical stretching would be smaller. Similarly we can argue that the stretching of the lower portions of the flux tube will not grow exponentially if these are less dense than the surrounding atmosphere (since $\Delta z < 0$). When both conditions (at the upper and lower boundaries of the flux tube) are brought together, we end up with an inhomogeneous flux tube. However, the lower boundary of the flux tube appears to be located near the continuum forming layers (Fig. 1, right panel), where the assumption of $\delta < 0$ is not completely justified.

Note that $B_{\mathrm{s}z}$ in Eq. (8) decreases strongly towards the outer penumbra, where the external field becomes weak and inclined ($B_{\mathrm{s}z} \sim 650\,\mathrm{G}$) and therefore $\Delta z/H_\mathrm{p} \sim -0.2/\delta$. Near the umbra however, $B_{\mathrm{s}z}$ reaches values as high as $1700\,\mathrm{G}$, and the vertical stretching is so large that the flux tube is likely to break or disappear. High spatial resolution images of the sunspot penumbra reveal that penumbral filaments pouring into the umbra often break into two individual filaments that continue moving inwards and form umbral dots. The details presented here offer a scenario that might account for this process.

4. Conclusions

We have shown, using simple estimates, that in a convectively stable atmosphere the vertical stretching of horizontal flux tubes, embedded in a penumbral field, is limited by buoyancy. It would be of considerable interest to use numerical simulations to confirm that the vertical stretching is compatible with the uncombed penumbral model.

References

Borrero, J. M., Lagg, A., Solanki, S. K., Frutiger, C., Collados, M., & Bellot Rubio, L. R. 2003, in ASP Conf. Ser. Vol. 286, High Resolution Solar Observations: Preparing for ATST, ed. A. Petsov & H. Uitenbroek (San Francisco: ASP), 235

Borrero, J. M., Solanki, S. K., Bellot Rubio, L. R., Lagg, A., & Mathew, S. K. 2004, A&A, 422, 1093

Borrero, J. M., Solanki, S. K., Lagg, A., Collados, M. 2005, A&A, 436, 333

Borrero, J. M., Solanki, S. K., Lagg, A., Socas-Navarro, H., & Lites, B. 2006, A&A, 450, 383

Langhans, K., Scharmer, G., Kiselman, D., Löfdahl, M., & Berger, T. 2005, A&A, 436, 1087

Martínez Pillet, V. 2000, A&A, 361, 734

Mathew, S., Lagg, A., Solanki, S. K., et al. 2003, A&A, 403, 695

Montesinos, B. & Thomas, J. 1997, Nat, 390, 485

Moreno-Insertis, F., & Spruit, H. C. 1989, ApJ, 342, 1158

Müller, D. A. N., Schlichenmaier, R., Steiner, O., & Stix, M. 2002, A&A, 393, 305

Rouppe van der Voort, L., Löfdahl, M. G., Kiselman, D., & Scharmer, G. B. 2004, A&A, 414, 717

Scharmer, G. B., Gudiksen , B. V., Kiselman, D., et al. 2002, Nat, 420, 151

Schlichenmaier, R. 2002, Astron.Nach., 323, 303

Schlichenmaier, R., & Collados, M. 2002, A&A, 381, 668

Schlichenmaier, R., & Solanki, S. K. 2003, A&A, 411, 257

Schlichenmaier, R., Jahn, K., & Schmidt, H. U. 1998a, A&A, 337, 897

Schlichenmaier, R., Jahn, K. & Schmidt, H. U. 1998b, ApJ, 483, L121

Schlichenmaier, R., Bruls, J., & Schüssler, M. 1999, A&A, 349, 961

Schlichenmaier, R., Müller, D. A. N., Steiner, O., & Stix, M. 2002, A&A, 381, L77

Solanki, S. K. 2003, A&ARv, 11, 153

Solanki, S. K., & Montavon, C. A. P. 1993, A&A, 275, 283

Spruit, H. C., & Scharmer, G. B. 2006, A&A, 447, 343

Sütterlin, P., Bellot Rubio, L. R., & Schlichenmaier, R. 2004, A&A, 424, 1049

Thomas, J., & Montesinos, B. 1993, ApJ, 407, 398

Westendorp Plaza, C., del Toro Iniesta, J. C., Ruiz Cobo, B., & Martínez Pillet, V. 2001a, ApJ, 547, 1148

Westendorp Plaza, C., del Toro Iniesta, J. C., Ruiz Cobo, B., et al. 2001b, ApJ, 547, 1130